

ARTICLE

Received 28 Aug 2015 | Accepted 13 Jun 2016 | Published 13 Jul 2016

DOI: 10.1038/ncomms12251

OPEN

Atomic scale observation of oxygen delivery during silver–oxygen nanoparticle catalysed oxidation of carbon nanotubes

Yonghai Yue^{1,2,*}, Datong Yuchi^{3,*}, Pengfei Guan^{4,*}, Jia Xu³, Lin Guo² & Jingyue Liu⁵

To probe the nature of metal-catalysed processes and to design better metal-based catalysts, atomic scale understanding of catalytic processes is highly desirable. Here we use aberration-corrected environmental transmission electron microscopy to investigate the atomic scale processes of silver-based nanoparticles, which catalyse the oxidation of multi-wall carbon nanotubes. A direct semi-quantitative estimate of the oxidized carbon atoms by silver-based nanoparticles is achieved. A mechanism similar to the Mars–van Krevelen process is invoked to explain the catalytic oxidation process. Theoretical calculations, together with the experimental data, suggest that the oxygen molecules dissociate on the surface of silver nanoparticles and diffuse through the silver nanoparticles to reach the silver/carbon interfaces and subsequently oxidize the carbon. The lattice distortion caused by oxygen concentration gradient within the silver nanoparticles provides the direct evidence for oxygen diffusion. Such direct observation of atomic scale dynamics provides an important general methodology for investigations of catalytic processes.

¹ LeRoy Eyring Center for Solid State Science, Arizona State University, Tempe, Arizona 85287, USA. ² Key Laboratory of Bio-inspired Smart Interfacial Science and Technology of Ministry of Education, Beijing Key Laboratory of Bio-inspired Energy Materials and Devices, School of Chemistry and Environment, Beihang University, Beijing 100191, China. ³ School for Engineering of Matter, Transport and Energy, Arizona State University, Tempe, Arizona 85287, USA. ⁴ Materials and Energy, Beijing Computational Science Research Center, Beijing 100193, China. ⁵ Department of Physics, Arizona State University, Tempe, Arizona 85287, USA. * These authors contributed equally to this work. Correspondence and requests for materials should be addressed to Y.Y. (email: yueyonghai@buaa.edu.cn) or to L.G. (email: guolin@buaa.edu.cn) or to J.L. (email: Jingyue.Liu@asu.edu).

Heterogeneous catalysis plays a major role in the production of energy and chemicals as well as in pollution control¹. Metal and metal-based nanoparticles (NPs), which are frequently used as active components for catalytic reactions, have captured broad attention in the past decades, especially for their potential applications in solving environmental problems^{2–4}. Development of highly efficient oxidation catalysts at low temperatures is crucial to dramatically reduce the emissions of particulates (mostly soot particles) into the environment⁵. Among many NP-based catalysts, Ag NPs hold many advantages due to their high reactivity and relatively low cost^{6,7}. As demonstrated recently, Ag/Ag₂O NPs possess lower activation energy^{8–11} and are assumed to be ideal catalysts for oxidizing carbonaceous materials. An interesting phenomenon of silver NP channelling graphene has been revealed which shows that graphene edges can dictate the morphology of NPs¹².

Carbon nanotube (CNT)¹³, a very important member of the family of carbonaceous materials, has been used as a model material for studying the oxidation processes of carbon-based materials^{14–16} because of its excellent mechanical and electrical properties and wide range of potential applications^{17–19}. Previous studies proposed an oxidation reaction model: the oxidation first occurs on the outside layer of a pristine CNT and the initiation temperature of the CNT oxidation depends on the wall thickness of the CNTs²⁰. However, the atomic scale understanding of the intrinsic nature of active sites is still elusive. For example, how do the oxygen molecules dissociate and how do they transport to the CNTs? It is important to understand the relationships among the atomic structures of Ag NPs, the atomic scale dynamics and the catalytic oxidation processes in order to develop better supported metal catalysts for desired catalytic properties.

In this communication, an aberration-corrected environmental transmission electron microscopy (AC-ETEM) is used to directly record the processes of silver-based NPs catalysed oxidation of multi-wall CNTs (MW-CNTs). The number of oxidized carbon atoms is directly estimated with a semi-quantitative method and thus the CO_x (including CO and CO₂) formation rate, which is equivalent to the turnover frequency (TOF), is obtained. Theoretical calculations, together with the direct AC-ETEM observation, suggest that a mechanism similar to the Mars–van Krevelen process dominates the oxidation process. The contact interfaces between the Ag/AgO_x NPs and the CNTs have the lowest oxygen concentration, while the exposed surfaces of the silver NPs possess the highest oxygen concentration. Such an oxygen gradient within the NPs provides the driving force to sustain the delivery of the oxygen atoms to the contact interfaces, between the Ag/AgO_x NPs and the CNTs, where the carbon atoms can be oxidized. The continuous evolution of the NPs, the Ag/CNT interfaces, and the oxidation of the CNTs are monitored and tracked. To the best of our knowledge, this is the first atomic scale observation of the oxidation of carbon materials by metal NPs. On the basis of the experimental observation, we propose that the oxygen molecules dissociate at the particle surfaces and the dissociated oxygen atoms diffuse through the NPs to reach the Ag/CNT interfaces and subsequently oxidize the CNTs. It is expected that such an approach to study catalytic reactions is general and may be extended to investigations of other important catalytic reactions.

Results

Sample preparation. The CNTs, prepared via a chemical vapour deposition method, were suspended in ethyl alcohol and a drop of the solution was then transferred to a molybdenum TEM grid coated with a thin holey-carbon film. The FEI Titan G2

AC-ETEM with a monochromator was employed to carry out the oxidation experiments. The environmental chamber can allow gas pressures up to ~20 mbar (ref. 21) (for more details, please visit <http://www.fei.com>). To acquire high-quality images, the TEM grid (without exposure to electron beam) was heated to 450 °C in 2 mbar O₂ for 45 min inside the ETEM to remove the contaminants on the surfaces of the CNTs. Many rounds of experiments confirmed that such a treatment does not oxidize the multi-wall CNTs (Supplementary Fig. 1 and Supplementary Note 1) and the contaminants were removed from the surfaces of the CNTs. To minimize the electron beam effects on the CNTs, all the experiments were conducted at 80 kV (ref. 22). A Gatan Inconel heating holder was used to control the temperature of the sample treatment and the catalytic oxidation reaction. All the images were recorded by a Gatan UltraScan CCD camera.

The pre-treated and clean CNTs were then loaded with AgNO₃ aqueous solution (Supplementary Note 2). The dried TEM grid was then put into the microscope chamber and 2 mbar of H₂ was allowed into the microscope chamber to reduce the sample at 250 °C for 2 h. During the reduction process, metallic Ag NPs were formed (Supplementary Figs 2 and 3). Some of the Ag-containing NPs attached to the CNTs were only partially reduced (Supplementary Note 3). After this treatment, various sizes of silver NPs were finely dispersed onto the surfaces of the CNTs. During the sample synthesis and treatment processes the electron beam was always blanked. Our experiences with ETEM showed that the high-energy electrons inside an electron microscope ionize oxygen molecules to generate oxygen radicals, which can easily oxidize carbonaceous materials even at ambient temperatures. Because of this limitation, we could not continuously observe the dynamic processes of the catalytic oxidation reaction with the electron beam on. We did, however, observe the same region, with atomic scale resolution, repeatedly for many cycles of the oxidation reaction by pumping out the oxygen for observation after each cycle of the oxidation reaction. In a strict sense, our observations were not exactly *in situ* due to the limitation by the electron beam-induced ionization of oxygen molecules. In this paper, we will denote such an experiment as quasi-*in situ*, since we tracked the same Ag/CNT interface for many oxidation cycles. Previous studies suggest that the initial oxidation of CNTs by Ag NPs starts at ~200 °C, much lower than the initial oxidation temperature of CNTs without the use of Ag NPs as catalysts^{3,5,23–25}. Therefore, a reaction temperature of 250 °C was chosen for the catalytic oxidation of our MW-CNTs.

Quasi-*in situ* oxidation experiments. The oxidation reaction was conducted inside the AC-ETEM at 250 °C for several cycles to examine the atomic scale dynamic oxidation process. After each cycle of the oxidation reaction, the residual oxygen inside the microscope chamber was thoroughly purged out and the sample temperature was maintained at ~250 °C. After purging and evacuation, the chamber vacuum pressure was <2 × 10⁻⁶ mbar and the electron beam was de-blanked to record images of the marked regions of interest. Figure 1a shows AC-ETEM images of CNTs after the sample treatment process revealing Ag NPs, with an average size of ~5 nm in diameter, decorating the surfaces of the CNTs. This initial examination served as a baseline for further monitoring of the structural evolutions of the Ag/CNT system. Several Ag NPs on the CNTs were selected as regions of interest and were monitored after each reaction cycle. After appropriate images were taken, the electron beam was blanked and the sample was oxidized in 2 mbar O₂ at 250 °C for 25 min. The regions of interest, before and after the oxidation reaction, were recorded at both low and high magnifications. Figure 1b shows the image, after 25 min oxidation reaction, of the same area as shown in

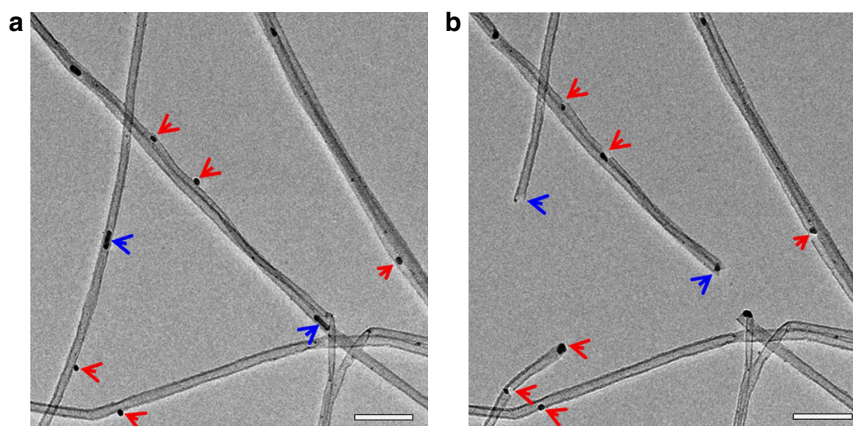


Figure 1 | TEM images of several MW-CNTs before and after oxidation. (a) TEM image shows several MW-CNTs before oxidation at 250 °C; (b) TEM image shows the same region as **a** but after oxidation at 250 °C for 25 min with 2 mbar O₂, clearly demonstrating the Ag catalysed oxidation of the MW-CNTs. Scale bar, 50 nm.

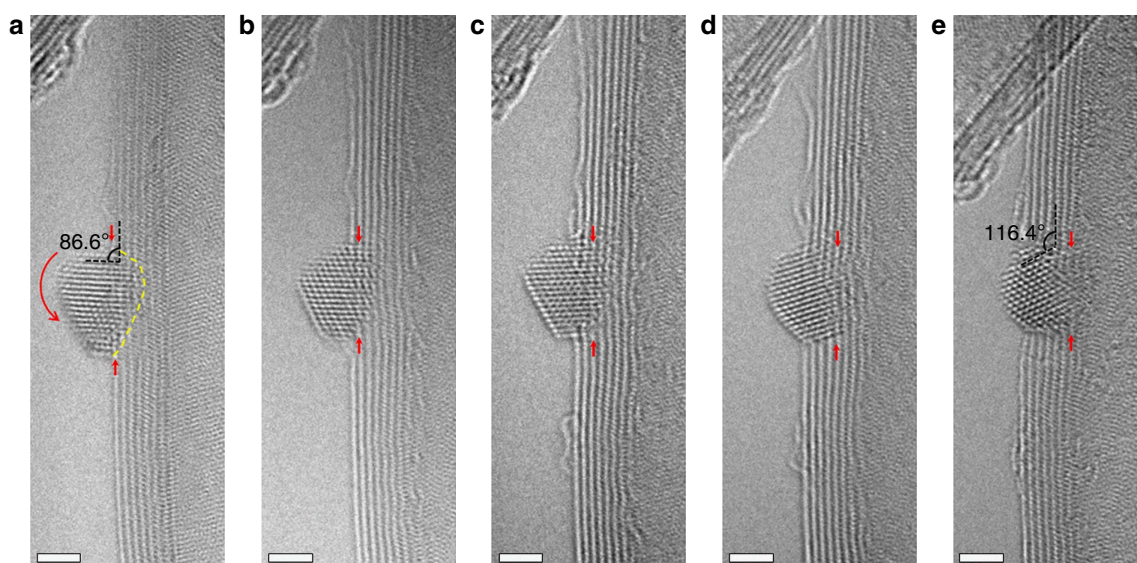


Figure 2 | A series of high-quality AC-ETEM images during the oxidation process. The oxidation reaction was conducted at 250 °C in 2 mbar O₂ with different oxidation times: (a) 0 s; (b) 300 s; (c) 600 s; (d) 900 s; and (e) 1,800 s. Scale bars, 2 nm. The two dashed black lines in **a** mark the angle between the Ag NP/MW-CNT system, which was used to monitor the rotation of the Ag NP. The curved red arrow denotes the rotation direction and the yellow dashed line marks the contact interface between the Ag NP and the MW-CNT.

Fig. 1a, clearly revealing the effect of the Ag NP during the catalysed oxidation of the CNTs. Furthermore, the effect of oxygen for the oxidation process was also studied as shown in Supplementary Fig. 4 and described in Supplementary Note 4. During the oxidation process, those carbon atoms which were directly in contact with the Ag NPs were oxidized to become CO or CO₂ (Supplementary Fig. 5 and Supplementary Note 5). Some NPs attached to the external surfaces of the CNTs (indicated by the red arrows in Fig. 1), others decorated the tips of the CNTs as shown in Supplementary Fig. 6 (Supplementary Note 6), and a small portion of the NPs were found inside the CNTs (indicated by the blue arrows in Fig. 1, Supplementary Figs 7 and 8, and Supplementary Note 7). During the oxidation process, the Ag NPs attached to the external surfaces of the CNTs either cut through or drilled holes into the CNTs, which can be used to improve the solubility of the CNTs²⁶.

Since the dynamic evolution of the oxidation reaction could not be directly observed because of the effects of electron beam-induced ionization of oxygen molecules (Supplementary Fig. 9 and Supplementary Note 8), a more elaborative set of

experiments were conducted to extract the atomic scale information of the oxidation processes. Figure 2 shows a series of atomic resolution AC-ETEM images demonstrating clearly the changes of the atomic structure caused by the oxidation reaction at 250 °C. By maintaining similar imaging conditions, the different phase-contrast AC-TEM images can be directly compared. Figure 2a shows a faceted Ag NP and the atomic layers of the MW-CNT before the oxidation reaction. However, after careful analysis of the lattice fringes of the 'Ag' NP in Fig. 2a, we concluded that it does not fit either the Ag metal or any existing phases of silver oxides (Supplementary Tables 1 and 2 and Supplementary Note 9), it is reasonable to assume that such ultra-small size Ag NPs can be oxidized easily. In another word, small Ag NPs are difficult to be reduced during the sample preparation process. Electron energy loss spectroscopy (EELS) results also show the existence of oxygen as shown in Supplementary Fig. 10 (see Supplementary Note 10 for more details). So, we can label these NPs as an AgO_x NP and the oxygen content within the NPs will be discussed later. The focus-dependence phase contrast of the AC-TEM images can be utilized to help locating the edges of

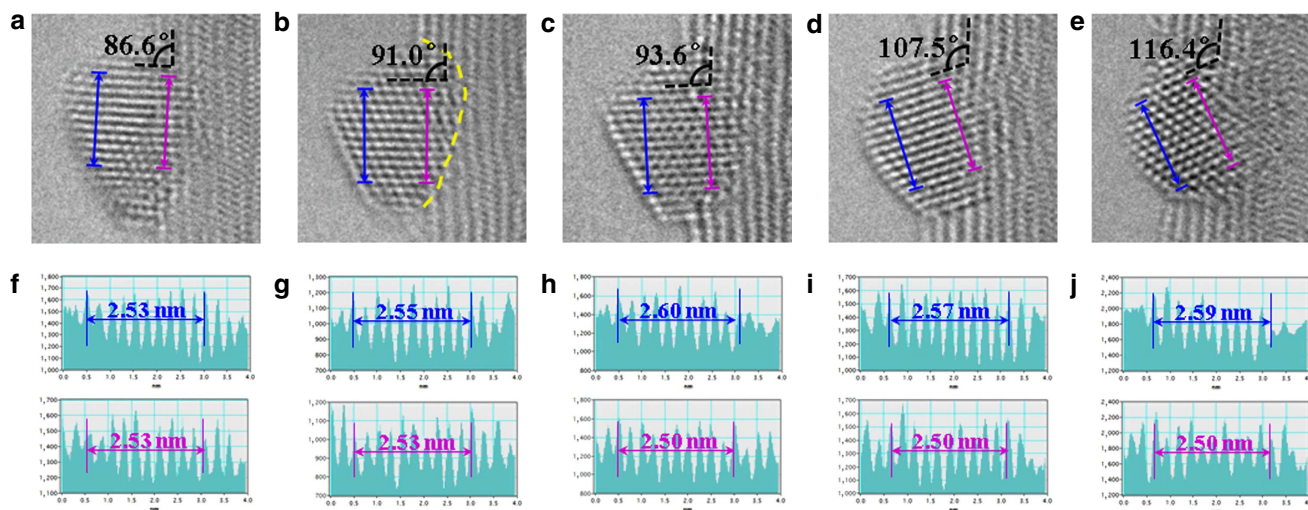


Figure 3 | Measurement of the change in lattice spacing induced by oxygen concentration gradient. (a–e) are enlarged images taken from Fig. 2; (f–j) are the measured d spacing of the outside and inner 10 interplanar spacing. The two black dashed lines marked the angle between the NP and the CNT, where the blue and pink double-head arrows marked the 10 outside (d_o) and inner (d_i) interplanar spacing within the NP.

the MW-CNTs (Supplementary Fig. 11 and Supplementary Note 11). Figures 2b–e were taken from exactly the same region but after an accumulated oxidation reaction of 300, 600, 900 s and 1,800 s, respectively. The red arrows indicate the reaction front, where the carbon atoms were in direct contact with the AgO_x NP. After the first oxidation cycle (2 mbar O_2 at 250 °C for the first 300 s), the outmost wall of the MW-CNT, which was in direct contact with the perimeter of the AgO_x NP, was oxidized, resulting in desorption of the carbon atoms as CO and/or CO_2 molecules. At the end of the second oxidation cycle (Fig. 2c, 2 mbar O_2 at 250 °C for the second 300 s), the AgO_x NP had catalysed the oxidation of two walls of the MW-CNT. Figure 2d shows the same sample area after the third cycle of oxidation (2 mbar O_2 at 250 °C for the third 300 s), clearly revealing the removal of four layers of the graphitic carbon and the advancement of the AgO_x NP into the MW-CNT. After another 900 s oxidation reaction (2 mbar O_2 at 250 °C for another 900 s), the AgO_x NP almost sank entirely into the interior of the MW-CNT and all the seven layers of the MW-CNT which had been crossed by the AgO_x NP were completely oxidized. Furthermore, by comparing Fig. 2a with Fig. 2e, a $\sim 30^\circ$ rotation of the NP, along the direction indicated by the curved red arrow (Fig. 2a) had occurred due to the asymmetric shape of the NP and the fact that carbon oxidation occurs only if the carbon atoms are in contact with the Ag atoms, the forward advancement of the AgO_x NP depends on the particle's shape and its dynamic interaction with the CNT. After the oxidation and the desorption of the carbon atoms, the side of the NP with larger contact area sank into the CNT faster than the side with smaller contact area, resulting in a torque force on the NP. Such a rotational precession of metal NP catalysts is of interest and may provide useful information on the nature of catalysed oxidation reactions. The tortuous track, created by AgO_x due to the oxidation of the CNT layers further suggests that the shape of the AgO_x NP controls its progression during the oxidation processes of the CNTs (Supplementary Fig. 12 and Supplementary Note 12).

To probe the nature of the oxidation mechanism, the structural change of the AgO_x NP was carefully analysed after each oxidation cycle. Figures 3a–e shows the enlarged image taken from Fig. 2a–e. A set of 10 interplanar spacings (as marked by the blue and pink arrows in Fig. 3a–e), d , were carefully measured from the outside of the NP (that is, the side farthest away from the NP/CNT contact interface indicated by the blue double heads

arrow), labelled as d_o , and the inner side (that is, the side closest to the NP/CNT contact interface, indicated by the pink double-head arrow), labelled as d_i , are shown in Fig. 3f–j. The d_o and d_i are, respectively, 2.53 and 2.53 nm in Fig. 3f; 2.55 and 2.53 nm in Fig. 3g; 2.60 and 2.50 nm in Fig. 3h; 2.57 and 2.50 nm in Fig. 3i; and 2.56 and 2.50 nm in Fig. 3j. The largest relative increase in lattice spacing of $\sim 4\%$ between d_o and d_i was demonstrated in Fig. 3h. The interplanar spacing of 0.35 nm of the CNTs was adapted as the internal calibration reference (see Supplementary Fig. 11a). We did not use the value of 0.34 nm (ref. 20) as the standard since the size effect²⁷ may play a roll as well. Regardless of the absolute value of the lattice spacing of the CNTs, we just used it as an internal reference. Since we measured many spacings and repeated the measurement for each oxidation cycle, it was estimated that the error in determining the lattice spacing should be $< 0.7\%$, far smaller than the measured lattice spacing differences between d_o and d_i . The EELS analyses of the NPs suggest the existence of O within these particles. Furthermore, according to the first-principles calculations (Supplementary Fig. 13 and Supplementary Note 13), the lattice spacing of the Ag-based FCC lattice can be influenced by the content of O and a $\sim 10\%$ lattice expansion can be expected for an oxygen content of $\sim 20\%$. The presence of different lattice values within a single NP, as measured experimentally, can be attributed to the different local oxygen concentration within the NP. This correlation is reasonable provided that O_2 molecules adsorb and dissociate on Ag which will be discussed later. By integrating all these experimental observations with theoretical calculations, we propose a working mechanism for the Ag NP catalysed oxidation of the CNTs. The oxygen atoms, originated from the dissociative adsorption of the gas phase oxygen molecules on the exposed surfaces of the Ag NP, diffuse into the Ag NP at moderate temperatures. The oxidation of the CNT carbon atoms requires the availability of the atomic oxygen at the NP/CNT contact interface, which is provided by the atomic oxygen within the Ag NP. During the oxidation process, the atomic oxygen at the NP/CNT contact interface is used to oxidize carbon and evaporate as CO_x ; while on the exposed surfaces of the NP, a constant supply of oxygen molecules is provided which dissociate and diffuse into the NP. Therefore a dynamic equilibrium of the oxygen concentration within the NP is established: Higher oxygen content near the exposed surfaces of the NP and lower oxygen content at the Ag/CNT interface, resulting in a gradient of atomic

oxygen within the NP. Therefore, during the catalytic oxidation of the CNTs, the AgO_x NPs act as a media to convert gas phase molecular oxygen into atomic oxygen and then supply them to the NP/CNT contact interfaces to oxidize the CNTs. In addition to the example demonstrated in Fig. 3, other examples were shown in the Supplementary Fig. 14 and Supplementary Note 14.

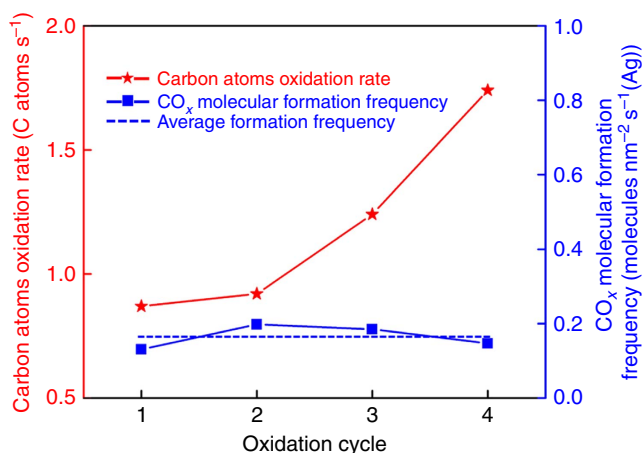


Figure 4 | Specific rate of carbon oxidation by the Ag NP shown in Fig. 2.

The red line shows the oxidation rate, the blue line shows the CO_x formation frequency per nm^2 of Ag, and the dashed blue line shows an average rate of the CO_x formation per nm^2 of the surface of the Ag NP.

The amount of the oxidized carbon atoms can be estimated from the AC-ETEM images provided that we use a reasonable model for the shape of the NPs. As shown in Fig. 2b, after the first oxidation cycle, the contact region between the NP and the outmost CNT wall was oxidized, the number of removed carbon atoms can be estimated from a simple model (Supplementary Fig. 15 and Supplementary Fig. 16, see more details in Supplementary Note 15 and Supplementary Note 16). If we assume that each layer of the CNT can be taken as a curved graphene layer with a planar density of ~ 38.17 atoms per nm^2 (Supplementary Fig. 15)^{3,28}, then the loss of the number of carbon atoms (due to formation of CO and/or CO_2) can be estimated as shown in Supplementary Table 3. The cumulative number of carbon atoms removed from the individual MW-CNT (Fig. 2) was quantitatively estimated to be 261, 275, 373 and 1,570 after the first oxidation cycle (300 s), the second cycle (total of 600 s), the third cycle (total of 900 s) and the fourth cycle (total of 1,800 s), respectively. The specific rates of the carbon oxidation by the individual Ag NP were estimated to be 0.87, 0.92, 1.24 and 1.74 carbon atoms per second, respectively (red line in Fig. 4). The increase of the specific rate with reaction time is a reflection of the increase in the Ag/CNT contact area when the Ag NP advanced during the oxidation process. If we assume that each surface Ag atom is catalytically active for the oxidation of the carbon then the TOF of the Ag active sites can be deduced (blue line in Fig. 4). Since the nature of active sites did not change after each oxidation cycle, the TOF should remain constant which was estimated to be $\sim 0.165 \text{ nm}^{-2} \text{ s}^{-1}$ (Ag) (dashed blue line in Fig. 4).

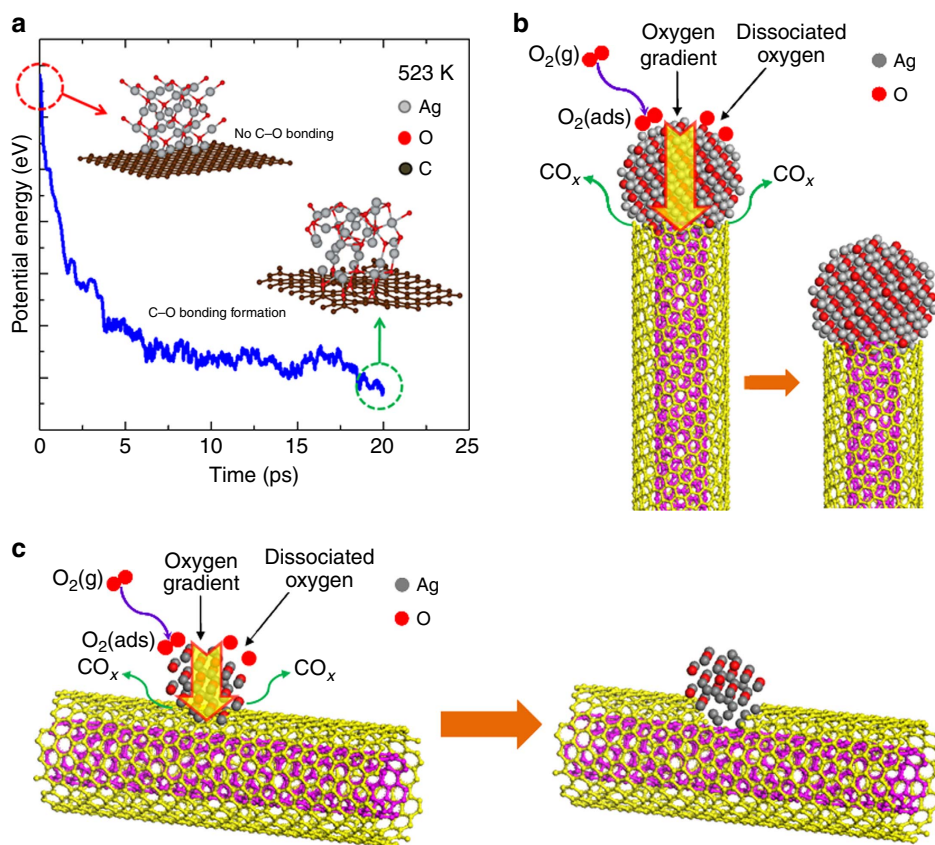


Figure 5 | Sketch map of the oxidation process. (a) *Ab initio* molecular dynamic simulation result. Here we use Ag_2O with a graphene support. The two insets were extracted from the simulation process. One is from the initial time marked by the red dashed circle and the other one is the final state after the C-O bonds formation marked by the green dashed circle. (b) The sketch map of the oxidation process for the case that the NP decorated the tip of the CNTs, while (c) shows the case the NP decorated the external surface of the CNTs, the yellow arrows in (b) and (c) show the oxygen concentration gradient.

Discussion

With the help of first-principles simulations, more insights into such silver-based NP catalysed oxidation processes can be acquired. According to the density functional theory (DFT) calculations (Supplementary Figs 17 and 18, and Supplementary Note 17), silver can readily reduce the energy barrier (~ 0.36 eV) in O_2 dissociation²⁹. Nevertheless, O_2 dissociation is strongly endothermic on graphene or CNT³⁰. It implies that the surfaces of silver NPs rather than the CNTs play the key role for O_2 dissociation at low temperatures, which explains why experimentally the carbon oxidation only occurred at the sites of CNTs that are in direct contact with Ag NPs. Furthermore, the DFT calculation shows that the oxidation of Ag surface is unstable due to the low thermal stability. The *ab initio* molecular dynamic simulation suggests that the O atom in Ag lattice could diffuse to the interfaces between Ag NPs and CNTs (Fig. 5a) resulting in oxidation of CNTs (Fig. 2). On the basis of previous studies, two catalytic mechanisms were proposed: Spillover mechanism³¹, suggesting that metal NPs activate O_2 molecules to produce active oxygen species which diffuse to the particle surface to oxidize the substrate³², and the analogy of the Mars–van Krevelen mechanism^{33,34}, implying that oxidation occurred via the movement of oxygen species within the lattice of the metal NPs. The AC-ETEM results (Figs 2 and 3) suggest that Ag NPs dissociate the gas phase oxygen molecules and then served as an oxygen-ion channel to deliver active oxygen species to the CNTs during the oxidation process, similar to the Mars–van Krevelen mechanism^{33,34}.

Electronic structure calculations suggested that the oxygen diffusion path lies midway between Ag atoms³⁵, and the presence of oxygen within the Ag NP can weaken the Ag–Ag bonds, giving rise to a higher probability for the oxygen species jumping from site to site³⁶ even at low temperatures^{37,38}. Figure 5b,c show the schematics illustrating the oxidation process of a silver oxide NP on the tip and the external surface of a CNT, respectively. As shown in Figure 5c, the O_2 is dissociated at the surface of NP and the NP acts as a dynamic reservoir for atomic O, providing active O atoms for CNT oxidation.

During the oxidation process, once the C atoms on the CNT were oxidized and CO_x molecules (marked in Fig. 5b,c) formed and released, an oxygen concentration gradient (as marked by the yellow arrows in Fig. 5b,c) would form inside the NP to establish a dynamic equilibrium: High concentration of oxygen species near the exposed surfaces of the AgO_x NPs and low oxygen concentration near the Ag/CNT interfaces. The oxygen species far from the contact area will supply this consumption by transiting oxygen species to the contact area, driven by the oxygen concentration gradient within the NPs. The continuous need of the atomic oxygen at the NP/CNT interfaces further demands the dissociative adsorption of the gas phase oxygen molecules ($O_{2(ads)}$) at the exposed surface of the NPs. The incorporation of the atomic oxygen increases the interplanar spacing of the silver NP³⁹. When the oxygen gas supply was stopped, the oxygen concentration near the exposed surfaces of the Ag NPs should be significantly reduced. Since the AC-ETEM images were acquired without the presence of the oxygen, the balanced oxygen concentration near the Ag/CNT interfaces, which is not enough to oxidize the carbon atoms of the CNTs was trapped inside the NP which causes the lattice expansion as evidenced by the AC-ETEM images.

This result provides very useful and original understanding of how the catalysed oxidation of carbon-based materials occurs on an atomic scale. Together with first-principles simulations, we reveal that an oxygen concentration gradient dominated oxidation process, which suggests that the oxygen molecules dissociate on the Ag NPs and diffuse through the Ag NPs to reach the Ag/CNT

interfaces and subsequently oxidize the carbon. Such direct observation of atomic scale dynamics provides an important general methodology not only for investigations of catalytic processes but also for improving advanced catalyst systems.

Methods

Quasi-*in situ* oxidation test. Before the oxidation test, the TEM grid with dispersed CNTs was heated in the AC-ETEM up to 450 °C and then 99.9999% ultrapure oxygen was introduced with a pressure of 2 mbar for 45 min to remove the surface contaminants. After such treatment, the CNTs were examined to make sure their cleanliness. The sample holder with the TEM grid was then taken out of the ETEM and a drop of $AgNO_3$ aqueous solution was loaded to the grid to deposit Ag-containing precursors to the CNTs and the support carbon films. The sample holder was then re-inserted back into the ETEM again and the whole system was reduced inside the microscope chamber with 2 mbar H_2 at 250 °C for 2 h, resulting in the formation of finely dispersed metallic Ag or AgO_x NPs. *In situ* oxidation reaction was performed with 2 mbar ultrapurity oxygen at 250 °C. The electron beam was blanked during the oxidation process in order to eliminate the electron beam-induced ionization effects²⁰. At the end of each oxidation cycle, the oxygen was purged out from the ETEM chamber while maintaining the sample temperature at 250 °C. The final chamber vacuum pressure was better than 2×10^{-6} mbar before the electron beam was de-blanked for examination. The same CNTs were located after each cycle of oxidation reactions. A total of four oxidation cycles were performed sequentially in order to extract information on the dynamic processes of the Ag catalysed oxidation of the CNTs. To minimize the electron beam effects on the CNTs, even without the presence of oxygen, all the experiments were conducted at 80 kV (ref. 22). The average dose used for imaging was $\sim 1250 e^- \text{ \AA}^{-2} s^{-1}$. We estimated that for each cycle of examination the total time for the CNTs exposed to the electron beam was about 80 s, resulting in a cumulative electron dose of $5 \times 10^5 e^- \text{ \AA}^{-2}$ for each cycle of examination. Repeated experiments confirmed that such operation conditions did not result in observable electron beam-induced damages of the Ag/CNT system.

Simulation details. Our calculations are based on DFT and use of a plane-wave, pseudopotential formalism^{40–42}. Exchange and correlation effects are included within the Perdew–Burke–Ernzerhof form of the generalized gradient approximation⁴³. For modelling the O_2 dissociation process at the Ag or graphene surface, we used the supercell geometry separated by a vacuum gap equivalent to 15 Å. To obtain the energy barrier of each dissociation pathway, calculations are performed with a plane-wave cutoff energy of 550 eV, and the same k-points (4×4) in the surface Brillouin zone was used for all structures. The total energy convergence criterion was 0.01 meV. All the atoms in the systems were fully relaxed until the largest residual force on any one was $< 0.02 eV \text{ \AA}^{-1}$. A Fermi surface smearing of 0.1 eV was used and the energy extrapolated to zero temperature. We included the spin-polarization energy in the calculation of the total energy of the free atoms and molecules. For the molecular dynamic simulation at infinite temperatures, the temperature was controlled by Noise–Hoove method and the time step was 2 fs.

Data availability. The authors declare that the data supporting the findings of this study are available within the article and its Supplementary Information files and from the corresponding author upon reasonable request.

References

1. Cargnello, M. *et al.* Exceptional activity for methane combustion over modular Pd@CeO₂ subunits on functionalized Al₂O₃. *Science* **337**, 713–717 (2012).
2. Wichmann, H. E. Diesel exhaust particles. *Inhal. Toxicol.* **19**, 241–244 (2007).
3. Tikhomirov, K., Krcher, O., Elsener, M. & Wokaun, A. MnOx–CeO₂ mixed oxides for the low-temperature oxidation of diesel Soot. *Appl. Catal. B* **64**, 72–78 (2006).
4. Wang, H. *et al.* *In situ* oxidation of carbon-encapsulated cobalt nanocapsules creates highly active cobalt oxide catalysts for hydrocarbon combustion. *Nat. Commun.* **6**, 7181 (2015).
5. Leino, A. R. *et al.* Low-temperature catalytic oxidation of multi-walled carbon nanotubes. *Carbon* **57**, 99–107 (2013).
6. Haneda, M. & Towata, A. Catalytic performance of supported Ag nanoparticles prepared by liquid phase chemical reduction for soot oxidation. *Catal. Today* **242**, 351–356 (2015).
7. Jiang, Z. J., Liu, C. Y. & Sun, L. W. Catalytic properties of silver nanoparticles supported on silica spheres. *J. Phys. Chem. B* **109**, 1730–1735 (2005).
8. Shimizu, K. I. *et al.* Carbon oxidation with Ag/ceria prepared by self-dispersion of Ag powder into nano-particles. *Catal. Today* **175**, 93–99 (2011).
9. Nanba, T., Masukawa, S., Abe, A., Uchisawa, J. & Obuchi, A. Morphology of active species of Ag/ZrO₂ for low-temperature soot oxidation by oxygen. *Catal. Sci. Technol.* **2**, 961–1966 (2012).
10. Miners, S. A., Rance, G. A., Torre, A. L., Kenny, S. M. & Khlobystov, A. N. Controlled oxidative cutting of carbon nanotubes catalysed by silver nanoparticles. *J. Mater. Chem. C* **2**, 8357–8363 (2014).

11. Shimizu, K., Kawachi, H. & Satsuma, A. Study of active sites and mechanism for soot oxidation by silver-loaded ceria catalyst. *Appl. Catal. B Environ.* **96**, 169–175 (2010).
12. Pizzocchero, F. *et al.* Graphene edges dictate the morphology of nanoparticles during catalytic channeling. *J. Phys. Chem. C* **118**, 4296–4302 (2014).
13. Iijima, S. Helical microtubules of graphitic carbon. *Nature* **354**, 56–58 (1991).
14. Ajayan, P. M. *et al.* Opening carbon nanotubes with oxygen and implications for filling. *Nature* **362**, 522–525 (1993).
15. Tsang, S. C., Harris, P. J. F. & Green, M. L. H. Thinning and opening of carbon nanotubes by oxidation using carbon dioxide. *Nature* **362**, 520–520 (1993).
16. Kosynkin, D. V. *et al.* Longitudinal unzipping of carbon nanotubes to form graphene nanoribbons. *Nature* **458**, 872–876 (2009).
17. Bachtold, A., Hadley, P., Nakanishi, T. & Dekker, C. Logic circuits with carbon nanotube transistors. *Science* **294**, 1317–1320 (2001).
18. Tans, S. J., Verschueren, A. R. M. & Dekker, C. Room-temperature transistor based on a single carbon nanotube. *Nature* **393**, 49–52 (1998).
19. Dai, H. J. Carbon nanotubes: opportunities and challenges. *Surf. Sci.* **500**, 218–241 (2002).
20. Koh, A. L., Gidcumb, E., Zhou, O. & Sinclair, R. Observations of carbon nanotube oxidation in an aberration-corrected environmental transmission electron microscope. *ACS Nano* **7**, 2566–2572 (2013).
21. Boyes, E. D. & Gai, P. L. Environmental high resolution electron microscopy and applications to chemical science. *Ultramicroscopy* **67**, 219–232 (1997).
22. Smith, B. W. & Luzzi, D. E. Electron irradiation effects in single wall carbon nanotubes. *J. Appl. Phys.* **90**, 3509–3515 (2001).
23. Landi, B. J., Cress, C. D., Evans, C. M. & Raffaele, R. P. Thermal oxidation profiling of single-walled carbon nanotubes. *Chem. Mater.* **17**, 6819–6834 (2005).
24. Miners, S. A., Rance, G. A., La Torre, A., Kenny, S. M. & Khlobystov, A. N. Controlled oxidative cutting of carbon nanotubes catalysed by silver nanoparticles. *J. Mater. Chem. C* **2**, 8357–8363 (2014).
25. Wang, C., Guo, S., Pan, X., Chen, W. & Bao, X. Tailored cutting of carbon nanotubes and controlled dispersion of metal nanoparticles inside their channels. *J. Mater. Chem.* **18**, 5782–5786 (2008).
26. Liu, J. *et al.* Fullerene pipes. *Science* **280**, 1253–1256 (1998).
27. Kiang, C. H., Endo, M., Ajayan, P. M., Dresselhaus, G. & Dresselhaus, M. S. Size effects in carbon nanotubes. *Phys. Rev. Lett.* **81**, 1869–1872 (1998).
28. Wei, J. K. *et al.* *In-situ* TEM imaging of the anisotropic etching of graphene by metal nanoparticles. *Nanotechnology* **25**, 465709 (2014).
29. Lončarić, I., Alducin, M. & Juaristi, J. I. Dissociative dynamics of O₂ on Ag (110). *Phys. Chem. Chem. Phys.* **17**, 9436–9445 (2015).
30. Nguyen, M. T. An *ab initio* study of oxygen on strained graphene. *J. Phys. Condens. Matter* **25**, 395301 (2013).
31. Conner, Jr W. C. & Falconer, J. L. Spillover in heterogeneous catalysis. *Chem. Rev.* **95**, 759–788 (1995).
32. Lorençon, E. *et al.* Thermal behavior of carbon nanotubes decorated with gold nanoparticles. *J. Therm. Anal. Calorim.* **105**, 953–959 (2011).
33. Doornkamp, C. & Ponc, V. The universal character of the Mars and Van Krevelen mechanism. *J. Mol. Catal. A Chem.* **162**, 19–32 (2000).
34. Lewandowski, M., Groot, I. M. N., Shaikhutdinov, S. & Freund, H. J. Scanning tunneling microscopy evidence for the Mars-van Krevelen type mechanism of low temperature CO oxidation on an FeO (111) film on Pt (111). *Catal. Today* **181**, 52–55 (2012).
35. Eberhart, M. E., Donovan, M. M. & Outlaw, R. A. *Ab initio* calculations of oxygen diffusivity in group-IB transition metals. *Phys. Rev. B* **46**, 12744 (1992).
36. Baird, J. K., King, T. R. & Stein, C. Diffusion of oxygen in silver. *J. Phys. Chem. Solids* **60**, 891–894 (1999).
37. MacLaren, J. M., Crampin, S., Vvedensky, D. D. & Pendry, J. B. Layer Korringa-Kohn-Rostoker technique for surface and interface electronic properties. *Phys. Rev. B* **40**, 12164 (1989).
38. Crampin, S., Vvedensky, D. D., MacLaren, J. M. & Eberhart, M. E. Electronic structure near (210) tilt boundaries in nickel. *Phys. Rev. B* **40**, 3413 (1989).
39. Yanase, A., Komiyama, H. & Tanaka, K. Adsorbate-induced lattice relaxation of small supported silver particles observed by an in situ X-ray diffraction technique. *Surf. Sci.* **226**, L65–L69 (1990).
40. Carlsson, J. M., Hanke, F., Linic, S. & Scheffler, M. Two-step mechanism for low-temperature oxidation of vacancies in graphene. *Phys. Rev. Lett.* **102**, 166104 (2009).
41. Kresse, G. & Furthmüller, J. Efficiency of *ab-initio* total energy calculations for metals and semiconductors using a plane-wave basis set. *Comput. Mater. Sci.* **6**, 15–50 (1996).
42. Blöchl, P. E. Projector augmented-wave method. *Phys. Rev. B* **50**, 17953 (1994).
43. Perdew, J. P., Burke, K. & Ernzerhof, M. Generalized gradient approximation made simple. *Phys. Rev. Lett* **77**, 3865 (1996).

Acknowledgements

This work was supported by the start-up fund of the College of Liberal Arts and Sciences of Arizona State University. We acknowledge the use of facilities in the John M. Cowley Center for High Resolution Electron Microscopy at Arizona State University. Y.Y. acknowledges National Natural Science Foundation of China (51301011); Research Fund for the Doctoral Program of Higher Education of China (20131102120053); Fundamental Research Funds for the Central Universities (YWF-16-GJSYS-25); and China Scholarship Council (No. [2014]-3012, 201406025060). P.G. thanks R. Su for help in the simulations; National Natural Science Foundation of China (51571011); the computational support from the Beijing Computational Science Research Center (CSRC) and the Center for Computational Materials Science, Institute for Materials Research, Tohoku University for supporting the use of the Hitachi SR11000 (model K2) supercomputing system.

Author contributions

Y.Y. and D.Y. conducted the *in situ* AC-ETEM oxidation experiments; P.G. carried out the theoretical simulations. These authors contributed equally to this reported research. J.X. prepared the AgNO₃ solutions. Y.Y., J.L. and L.G. designed the project and guided the research. Y.Y., P.G., J.L. and L.G. wrote the manuscript. All authors contributed to the revision of the paper.

Additional information

Supplementary Information accompanies this paper at <http://www.nature.com/naturecommunications>

Competing financial interests: The authors declare no competing financial interests.

Reprints and permission information is available online at <http://npg.nature.com/reprintsandpermissions/>

How to cite this article: Yue, Y. *et al.* Atomic scale observation of oxygen delivery during silver-oxygen nanoparticle catalysed oxidation of carbon nanotubes. *Nat. Commun.* 7:12251 doi: 10.1038/ncomms12251 (2016).



This work is licensed under a Creative Commons Attribution 4.0 International License. The images or other third party material in this article are included in the article's Creative Commons license, unless indicated otherwise in the credit line; if the material is not included under the Creative Commons license, users will need to obtain permission from the license holder to reproduce the material. To view a copy of this license, visit <http://creativecommons.org/licenses/by/4.0/>

© The Author(s) 2016